Reconciling the Pauling bond length picture and Vegard's law in a mixed crystal: An x-ray fluorescence holographic study

Shinya Hosokawa,[1,*] Naohisa Happo,[2] and Kouichi Hayashi[3]
[1]*Center for Materials Research Using Third-Generation Synchrotron Radiation Facilities, Hiroshima Institute of Technology, Hiroshima 731-5193, Japan*
[2]*Graduate School of Information Sciences, Hiroshima City University, Hiroshima 731-3194, Japan*
[3]*Institute of Materials Research, Tohoku University, Sendai 980-8577, Japan*
(Received 24 September 2009; published 26 October 2009)

In order to bridge experimental results for the atomic structure in mixed crystals between x-ray diffraction showing a Vegard's law and x-ray absorption fine structure spectroscopy indicating preservations of each Pauling's bond length, an x-ray fluorescence holography (XFH) experiment was carried out on $Zn_{0.4}Mn_{0.6}Te$ single crystal for drawing a three-dimensional atomic image around the Zn atom. The XFH image intensities of Te atoms in $Zn_{0.4}Mn_{0.6}Te$ with respect to the reference ZnTe are almost constant beyond the five chemical bonds from the central Zn atom, while the nearer Te atomic images are much weaker, indicating that the Pauling's bond length interconnects with Vegard's law at about five chemical bonds. The randomness of the atomic positions is well explained by a *locomotive wheel* atomic configuration model.

DOI: 10.1103/PhysRevB.80.134123 PACS number(s): 61.50.−f, 61.66.Fn

I. INTRODUCTION

Needless to say, it is very important to know atomic structure of materials for understanding their nature. If the sample is a perfect single crystal, the single crystal structure analysis using x-ray or neutron diffraction (XD or ND) is the perfect method, which detects *periodicity* of single crystal. Even if a single crystal has an extremely large size of the unit cell, such as protein crystals, difficulties can nowadays be solved using intense synchrotron radiation sources. Powder diffraction method is also a powerful tool to determine the crystal system and its lattice constants even for polycrystalline materials. Although a proper model is required, it is possible to determine detailed positions of the individual atoms in its unit cell.

If the sample is not a perfect crystal, e.g., modified by mixing of other elements, the above methods cannot determine the positions of the elements perfectly, because the perfect periodicity of the atomic structure is broken and it comprises a randomness in the atomic positions. As a result, the unit cell size of the crystal becomes in principle infinite. In recent days, most of functional materials are made up of mixing of many elements, which categorize such imperfect crystals. Thus, one should recognize that the diffraction is not the perfect method for investigating their atomic structures.

An alternative method for obtaining atomic structures is x-ray absorption fine structure (XAFS), which is widely used for investigating *local* atomic structure around a specific element, and can be adopted to even disordered materials. From this method, however, one can obtain only one-dimensional information, i.e., directionally averaged pair distribution functions. Moreover, the obtained information is usually limited to the second or third neighboring atoms due to the short mean-free path of x-ray excited photoelectrons.

Due to the difference of spatial scales surveyed by the XD (or ND) and XAFS measurements, differences between the results were reported even in the first nearest neighbor distances of mixed crystal. For example, mixed crystals of diluted magnetic semiconductors $Zn_{1-x}Mn_xTe$, being taken up in this paper, have such different reports between them. Figure 1 shows the concentration dependence of the nearest neighbor distance obtained from XD[1] and XAFS[2] for $Zn_{1-x}Mn_xTe$. From the lattice constants, a, obtained from XD results showing sharp Bragg peaks even for the mixtures,[1] the bond lengths were calculated for their zinc-blende structure, $\sqrt{3}a/4$, which are given by the triangles in Fig. 1. As clearly seen in the figure, the XD results show the Vegard's law[3] behavior, i.e., it linearly changes with x. On the contrary, results from the XAFS experiments given by the circles indicate that the nearest neighbor distance changes very little with x; it looks largely keeping the Pauling's bond lengths[4] of Zn-Te and Mn-Te different by 0.007–8 nm.

The same discrepancies were widely reported in many mixed crystals, such as $Si_{1-x}Ge_x$,[5] $Ga_{1-x}In_xAs$,[6–9] $ZnSe_{1-x}Te_x$,[10,11] $Cd_{1-x}Zn_xTe$,[12] $Cd_{1-x}Mn_xTe$,[13,14] and ionic solid solutions.[15,16] Several attempts were carried out to infill the experimental gap of the long-range XD data and the local

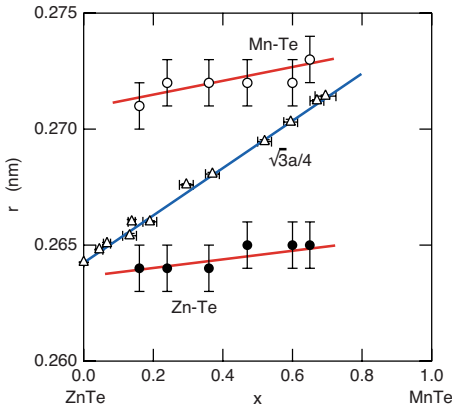

FIG. 1. (Color online) The concentration dependence of the nearest neighbor distance obtained from XD (triangles)[1] and XAFS (circles)[2] results for mixed crystals of $Zn_{1-x}Mn_xTe$.

XAFS results, by proposing suitable models[5,11,14] or by extending the experimental survey range to shorter for XD[8,9] or longer for XAFS.[11,16] In order to make the proper connection between them, however, a new experiment is necessary to investigate intermediate-range order in mixed crystal. For this, we think that x-ray fluorescence holography (XFH) is a good tool, which was developed by Tegze and Faigel[17,18] as a reliable method of structure characterization.

XFH is a technique that allows one to obtain a three-dimensional (3D) image of local atomic arrangement around a specific fluorescing element. This technique can explicitly determine the position of the constituent atoms with respect to a specific element emitting fluorescent x-rays with no special atomic model. In this paper, we clarify where Pauling's bond length interconnects with Vegard's law in a mixed crystal by measuring Zn K_α XFH for the $Zn_{0.4}Mn_{0.6}Te$ mixed crystal.

II. EXPERIMENTAL PROCEDURE

The $Zn_{0.4}Mn_{0.6}Te$ and the reference ZnTe single crystal samples were grown by a Bridgeman method. The sample with the (110) surface and a surface size of about 5 $\times 5$ mm^2 was placed on the two-axes table of a diffractometer installed at the beamline BL6C of the Photon Factory at KEK, Tsukuba, Japan. The measurements were performed by rotating the two axes, $0° \leq \theta \leq 70°$ in steps of 1° and $0° \leq \phi \leq 360°$ in steps of 0.35°, of the sample, and detecting small intensity variations of about 0.1 % in fluorescent x-ray intensity with angles. The Zn K_α fluorescent x-rays were collected using an avalanche photodiode detector with a cylindrical graphite-crystal energy analyzer. Each scan took about 11 h. Details of the experimental setup were given elsewhere.[19,20]

The holograms were recorded at nine incident x-ray energies of 11.0–15.0 keV in steps of 0.5 keV. The hologram oscillation data were obtained by subtracting the background from the normalized intensities. An extension of the hologram data to the 4π sphere was carried out using crystal symmetry of cubic zinc-blende structure and the measured x-ray standing waves (XSW) lines. Figure 2 shows an example of the hologram measured at the incident x-ray energy of 11.5 keV. The radical and angular directions indicate θ and ϕ, respectively. Shadow lines are observed in the pattern shown as arrows, whose indices are given in the figure. These lines originate from XSW. Since a Fourier transform of the XFH data at a single incident x-ray energy produces false twin images, a 3D atomic image was constructed using Barton's algorithm[21] by superimposing the holograms with nine different incident x-ray energies, which can highly suppress the false images.

III. RESULTS

Figures 3(a) and 3(b) show the 3D atomic images of $Zn_{0.4}Mn_{0.6}Te$ and ZnTe, respectively, around the central Zn atom. Also, the images on the (110) plane were preliminary shown in Fig. 1 of Ref. 22. The images of the first neighbor Te atoms appear at the proper positions assumed by the

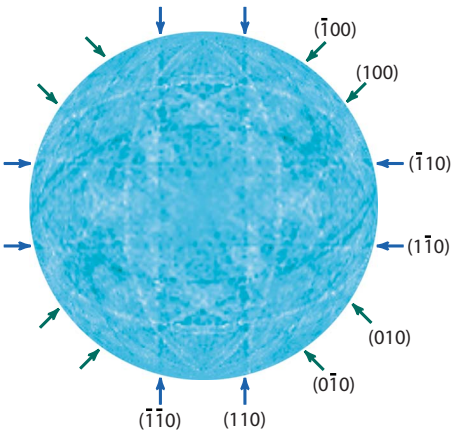

FIG. 2. (Color online) An example of a 4π full symmetrized hologram measured on $Zn_{0.4}Mn_{0.6}Te$ at 11.5 keV. See the text for details.

XAFS result[2] within the error bars. As regards the second neighbor cation (Zn or Mn) atoms (two bonds from the central Zn atom), since the scattering x-ray signals from atoms with low atomic numbers are highly suppressed due to the small number of core electrons, the images are hardly visible in $Zn_{0.4}Mn_{0.6}Te$ mixed crystal. On the contrary, the third neighbor Te atoms (three bonds) can be clearly observed.

Since the magnitude of XD signal strongly depends on the atomic form factor or the atomic number, the XD results are suggested to be mainly influenced by the arrangement of the Te sublattice. The images on the (001) plane are depicted in Fig. 4(a) for $Zn_{0.4}Mn_{0.6}Te$ and (b) ZnTe, where only Te atoms locate, and the central Zn atoms are beneath the center of the figures by $a/4$. For the reference, the zinc-blende crystal structure is depicted in Fig. 4(c). The large circles indicate Te atoms, and the small circles Zn or Mn atoms. The thick circles locate on a (001) plane, and correspond to the atomic images in (a) and (b).

A careful comparison of the images between the $Zn_{0.4}Mn_{0.6}Te$ and ZnTe crystals reveals that the images of the

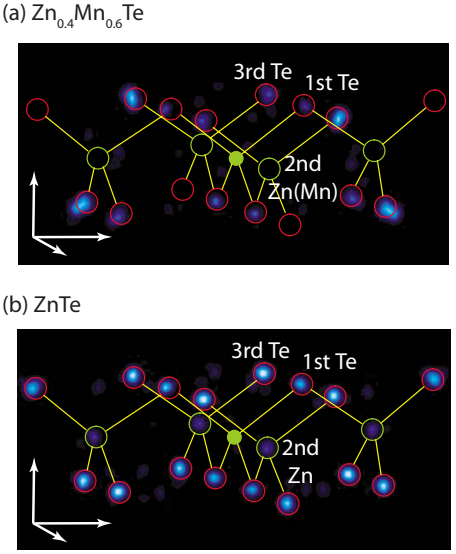

FIG. 3. (Color online) The 3D image intensities of Te atoms in (a) $Zn_{0.4}Mn_{0.6}Te$ and (b) ZnTe. See the text for details.

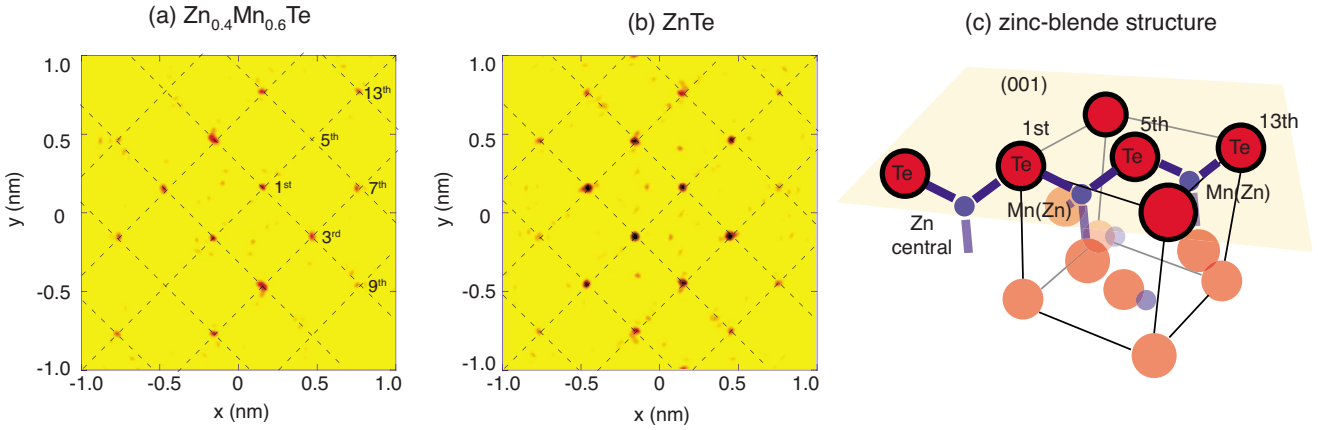

FIG. 4. (Color online) Atomic images around the central Zn atoms on the (001) plane for (a) $Zn_{0.4}Mn_{0.6}Te$ and (b) ZnTe. The crosses of the dashed lines are the positions of the zinc-blende crystal structure taken from the XD data.[1] (c) The zinc-blende structure of $Zn_{0.4}Mn_{0.6}Te$ mixed crystal.

first and fifth neighboring Te atoms (one and three bonds, respectively) in the $Zn_{0.4}Mn_{0.6}Te$ mixed crystal are much weaker than those in the ZnTe perfect crystal. However, the most important result of the present XFH experiment is that the images of the thirteenth neighboring atoms (five bonds) come back to be much stronger. Moreover, the further distant Te atoms also show clear images. In order to show them clearer, the image intensities of Te atoms in $Zn_{0.4}Mn_{0.6}Te$ and ZnTe are given in Fig. 5(a). Their intensity ratios are also given below the marks in the figure. Although the ratio values are rather scattered, those for near neighbor Te atoms below 0.8 nm range about 0.5–0.6. On the contrary, those for the distant Te atoms beyond 0.8 nm approach a large value of 0.7–0.8. Thus, the Te sublattice keeps the long-range periodicity.

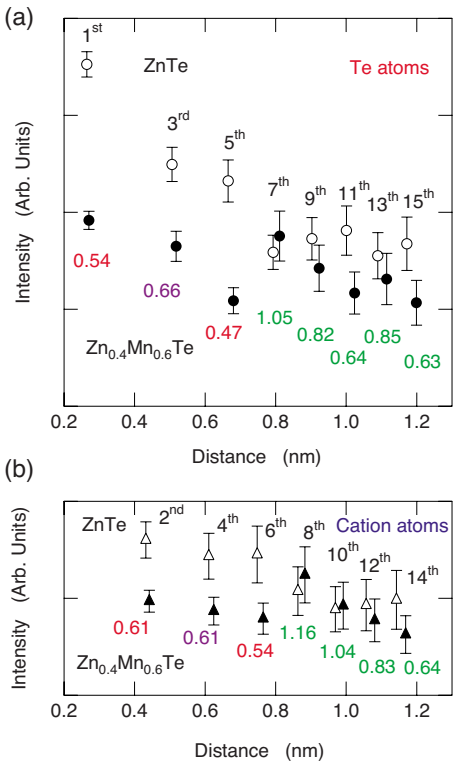

FIG. 5. (Color online) The image intensities of (a) Te atoms and (b) cation atoms in $Zn_{0.4}Mn_{0.6}Te$ (closed marks) and ZnTe (open marks). The ratios are given below the marks. See the text for details.

The image intensity ratios were also obtained for the cation (Zn or Mn) sublattice. The image intensities of cation atoms in $Zn_{0.4}Mn_{0.6}Te$ and ZnTe are given in Fig. 5(b). Note that compared to the Te image intensity, the scale of the cation intensity is much enhanced in the figure, and the real cation intensities are much weaker than the Te image intensity in (a). The ratios for the cations intensities show a tendency similar to those for the Te atoms, i.e., those for near neighbor cation atoms below 0.8 nm (from second to sixth neighbors with two-four chemical bonds) range about 0.6. Since the scattering intensity of Mn atoms during the holographic process is weaker than that of Zn atoms, the intensity value of the cation sublattice in the $Zn_{0.4}Mn_{0.6}Te$ mixed crystal becomes weaker by about 10% than that in ZnTe even if no spatial randomness is induce by the mixing. Thus, the reduce of the intensity by mixing is about 0.65, which is still similar to that in the Te sublattice. On the contrary, those for the distant cation atoms beyond 0.8 nm approach large values of almost unity, although the errors for these ratios are very large because the images of the cations are much weaker than those of the Te atoms. Nevertheless, the cation sublattice looks also keeping the long-range periodicity.

IV. DISCUSSION

For the first neighbor Te image, since the XAFS results revealed that the Zn-Te bond length is fixed to be almost the Pauling's value,[4] the randomness of the first neighboring Te positions appears only in the angular direction, which substantially reduces its image intensity. The position of the fifth neighboring Te atoms (three bonds) is also fluctuated because they connect with either Zn or Mn atoms with different bond lengths, i.e., the position vacillates radially as well as angularly. Thus, the smaller ratio value for the fifth neighboring Te atoms (three bonds) may be reasonable qualitatively.

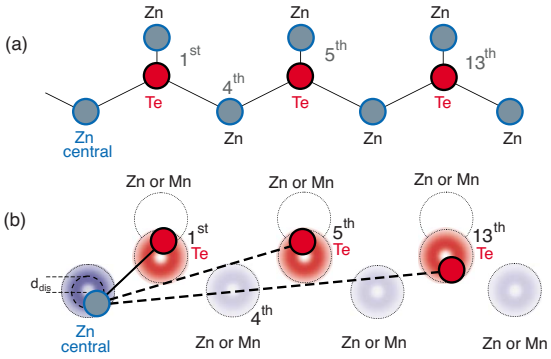

FIG. 6. (Color online) Schematic views of (a) the zinc-blende structure of ZnTe along the ⟨110⟩ direction and (b) the *locomotive wheel* model for $Zn_{0.4}Mn_{0.6}Te$.

Below, the relation of the randomness of the atomic positions and the present XFH data will be analyzed quantitatively. The resolution of the atomic images obtained by XFH is about 0.05 nm.[18] Therefore, separated images cannot be observed if the difference of the atomic positions is within 0.05 nm. However, the intensity of holographic image is highly related to the randomness of the atomic positions, and can be calculated theoretically.

The simplest assumption for the atomic position randomness is that the central Zn atom is fixed and the neighboring atomic positions have a spherical Gaussian distribution. Following the scattering process in the inverse XFH mode, the atomic image intensities were simply calculated by using the atomic form factors and varying the standard deviation of the Gaussian, σ, for the atomic positions. However, it gives only an individual σ value for each neighbor, which does not solve the question why the XFH intensities of the near neighbor atoms are largely suppressed.

Since the XD result shows the sharp Bragg peaks even for the mixtures,[1] we started to consider a model by assuming that each atom locates around its averaged lattice position. Figure 6 shows the schematic views of (a) the perfect zinc-blende structure of ZnTe and (b) the model for $Zn_{0.4}Mn_{0.6}Te$ along the ⟨110⟩ direction. In this model, each atom in $Zn_{0.4}Mn_{0.6}Te$ is assumed to locate always on a sphere with a distance from the average position, d_{dis}, and fluctuate from the sphere with a proper mean-square displacement obtained from the XAFS result.[2] From its shape, we named this structural model as a *locomotive wheel* model.

The calculations of the image intensity were made at the atomic distances from the central Zn atom of 0.3, 0.6, and 0.9 nm, and almost the same d_{dis} dependences were obtained. Thus, the average is given in Fig. 7. The solid curve shows the d_{dis} dependence of the image intensity of Te atoms normalized with respect to the $d_{dis}=0$ values. i.e., the values of the perfect ZnTe crystal with the same mean-square displacement. The averaged intensity ratio for the distant Te atoms beyond the seventh is about 0.73, which corresponds to d_{dis} ~ 0.014 nm as indicated the solid circle on the solid curve. This value is reasonable because the bond lengths of Zn-Te and Mn-Te differ from each other by 0.007–8 nm.

The atomic positions of the first neighboring Te should fluctuate mainly angular direction or two-dimensional (2D).

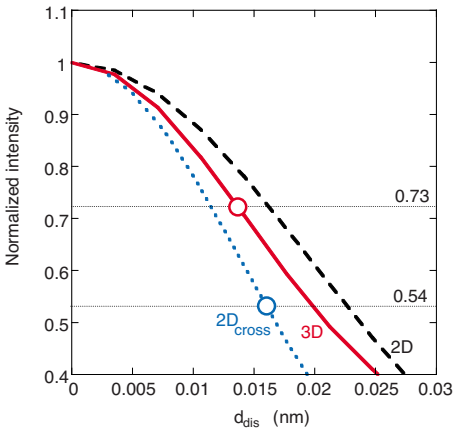

FIG. 7. (Color online) The d_{dis} dependence of the normalized XFH image intensity of the Te atoms.

In order to include such a constraint of the Pauling's bond length in this model, the first nearest neighbor distance and the mean-square displacement of Zn-Te bond obtained from the XAFS study were used for the radial constraints. The dashed curve in Fig. 7 shows the result of the calculation by including the above 2D constraint. The theoretical ratio from this 2D calculation with the same d_{dis} value is about 0.8, which is much larger than the present XFH result of 0.54. This is due to the lack of a further constraint in the geometrical configuration of atoms.

If the central Zn atom shifts toward a direction from the central position, the first neighbor Te atom may likely shift toward the opposite direction to fill the free volume induced by the movement of the Zn atom, as shown in the first neighbor Te atom in Fig. 6(b). This feature was included in the 2D model by adding a new constraint that the first neighbor Te atom should locate in the opposite angular side, i.e., a cross configuration with respect to the average Zn-Te bond. This constraint makes the angular randomness of the Zn-Te bond wider by almost twice. The dotted curve in Fig. 7 shows the result of 2D calculations with this cross constraint ($2D_{cross}$). As indicated by the circle on the dotted curve, the experimental ratio of 0.54 corresponds to the d_{dis} value of 0.016 nm, which is similar to $d_{dis}=0.014$ nm for the far distant Te lattice.

For the fifth neighboring Te atoms (three bonds), the image intensity ratio is 0.47, corresponding the d_{dis} value of about 0.022 nm in this model. This is much larger than the d_{dis} values for the first and distant Te atoms, and further local constraints for the atomic configuration may be still necessary for the fifth neighbor Te (three bonds).

In order to examine the validity of this model, we calculated the XD and XAFS spectra using this model and compared to the experimental results. Small circles in Fig. 8(a) show the Fourier back transformed spectrum of the main peak range in the Fourier transform, $F(r)$, of the Zn K-edge XAFS function, $k^3\chi(k)$,[2] indicating the contributions of the first neighbor Te atoms in the XAFS function. Solid curve in Fig. 8(a) represents the calculated XAFS curve for the nearest neighbor Te atoms by using a FEFF8 package[23] with the nearest-neighbor distance and mean-square displacement values used for the *locomotive wheel* model. Since the model

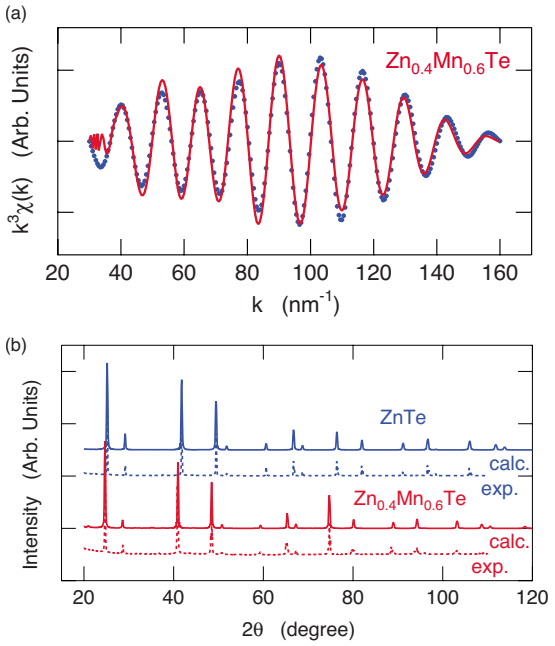

FIG. 8. (Color online) The calculated (solid curves) and experimental (dashed curves) curves of (a) XAFS and (b) XD spectra with Cu K_α radiation. See the text for details.

was based on the XAFS data, the agreement with the XAFS data is, of course, very good. The solid curves in Fig. 8(b) show the calculated XD spectra with the Cu Kα radiation obtained from the zinc-blende structure of ZnTe (upper) and the *locomotive wheel* model for $Zn_{0.4}Mn_{0.6}Te$ mixed crystal (lower) provided that d_{dis} is the same value of the experimental result for the first neighbor Te, 0.016 nm, together with the experimental results given by the dashed curves. The calculated XD spectra show clear Bragg peaks with the positions of Vegard's law, and coincide well with the experimental data in both the peak positions and heights. Thus, the *locomotive wheel* model can explain the results of all the existing experimental results of the XD and XAFS, as well as almost the present XFH data except the fifth neighbor Te atoms (three bonds).

In addition, a detailed observation of the XFH result in Fig. 5(a) indicates that the recovering or the self-organizing to the Vegard's law does not happen isotropically. The ratios of the third (three bonds) and seventh (five bonds) neighboring Te atoms, which are not on the ⟨110⟩ direction, are larger than those of the fifth (three bonds) and the thirteenth (five bonds) neighboring Te atoms, respectively. This result can be easily explained that the dihedral angle can distort more easily than the bond length and the bond angle.

More than two and a half decades ago, local structure of a zinc-blende semiconductor $Ga_{1-x}In_xAs$ was investigated by Mikkelsen and Boyce[6,7] using the XAFS measurements to detect the deviation from the virtual crystal approximation (VCA) crystal expected by XD measurements. Their detailed XAFS analysis revealed the following: 1) A significant deviation from the Vegard's law exists in the nearest-neighbor cation-anion distances, varying only slightly with x. 2) The second-neighbor cation-cation distances are approximately equal to the average distance as obtained by the XD measurements. 3) On the other hand, the second-neighbor anion-anion distribution is bimodal with the As-Ga-As and As-In-As distances close to those in the pure compounds GaAs and InAs, respectively. Very similar results are also obtained by them in the anion substituted zinc-blende alloy $ZnSe_{1-x}Te_x$,[10] or even in the ionic solid solutions.[15]

Based on these XAFS results, they drew an analogy between the $Ga_{0.5}In_{0.5}As$ and the chalcopyrite (ABX_2, e.g., $CdGeAs_2$ or $ZnSnAs_2$) crystal structures. In the chalcopyrite structure, the cations occupy face-centered tetragonal sites, which is very similar to two zinc-blende cubic lattice positions, i.e., the cation sublattice shows a VCA sublattice. On the other hand, the anion atoms are displaced from their respective *fcc* sublattice along the ⟨100⟩ or ⟨010⟩ directions, which results in bimodal cation-anion bond lengths. Although this analogy can adopt only to the 50:50 alloy $Ga_{0.5}In_{0.5}As$, it is a good starting point to make bridges between the XD and XAFS results.

Barzarotti and co-workers measured XAFS on mixed crystals of diluted magnetic semiconductors $Cd_{1-x}Mn_xTe$,[13,14] having the same zinc-blende crystal structure, and obtained the bimodal distribution of the nearest-neighbor distances similar to that in $Ga_{1-x}In_xAs$, although the second-neighbor analysis was not performed due probably to the limited k range of the Cd L_{III}, Mn K, and Te L_{III} XAFS functions. A model was developed by assuming that the cation sublattice remains undistorted with the VCA sublattice value, and by considering all the possible coordination around an anion in the alloy by displacing the anion from the central position only in the single tetrahedron, which does not affect the next and further distant tetrahedra. This model can be applied to any compositions of the mixed crystals in contrast to the Mikkelsen-Boyce's chalcopyrite analogy for the $Ga_{0.5}In_{0.5}As$ mixed crystal.[7] They applied this model to the zinc-blende type mixed crystals, not only to the $Cd_{1-x}Mn_xTe$ diluted magnetic semiconductors but also to the $Ga_{1-x}In_xAs$ mixed semiconductors, and explained well the bimodal distributions of the cation-anion nearest-neighbor distances and the randomness of the local distortions of the anion sublattice obtained by the XAFS experiments, although the latter was not examined in $Cd_{1-x}Mn_xTe$.

From the XD side, an attempt to bridge the experimental results of Pauling's bond length by XAFS and Vegard's law by ordinary XD was performed by Petkov *et al.*[8] on the $Ga_{1-x}In_xAs$ mixed crystals. Nearest- and higher-neighbor distances as well as bond length distributions were obtained from high real-space resolution atomic pair distribution functions (PDF) by high-energy XD measurements. In these PDFs, the first peak is clearly resolved into two subpeaks corresponding to the Ga-As and In-As bond lengths.[8] The evolution of the bond lengths with changing Ga(In) composition gives good agreement with the XAFS results.[6,7] They concluded that the above model by Balzarotti *et al.*[13,14] does not correctly explain the shape of the first peak region in the measured PDF. Moreover, the PDF shows that the higher neighbor structure exhibits Vegard's law type behavior by 1 nm.

It, however, seems to be very difficult to obtain information from the PDF data where the Pauling's bond length seen at the local atomic configuration interconnects with Vegard's

law observed at the distant periodic range. It should be noted that the present XFH results clearly reveal the sudden interconnection occurring at about five chemical bonds of 0.7–8 nm in the $Zn_{0.4}Mn_{0.6}Te$ mixed crystal.

Jeong *et al.*[9] modeled the local atomic displacements by a relaxed supercell of the alloys using a Kirkwood potential with nearest-neighbor bond stretching and bond angle bending forces. This model successfully reproduces the shape of the bimodal in the first peak region of the measured PDF. Another excellent advantage of their model is that three-dimensional the cation and As ensemble average distributions can be obtained to clarify the distortion probabilities of each sublattice experimentally at the distant periodic limit. It was found that the As atom displacements are large with about 0.01 nm in space for the $Ga_{0.5}In_{0.5}As$ alloy (similar space range to the d_{dis} value of 0.014 nm for the Te sublattice in our *locomotive wheel* model), and highly anisotropic along the ⟨100⟩ and ⟨111⟩ directions, which can be easily understood by the tetrahedral cluster model by Balzarotti *et al.*[13,14] In contrast to the model by Balzarotti *et al.*, significant static disorder associated with the cation sublattice (about 60% of the As sublattice) is also obtained from the above RDF analysis.

From the present XFH experiment, the image intensity ratios, reflecting the positional randomness of each atom, seem to have no significant differences between the cation and Te sublattices as shown in Fig. 5, although the cation image intensities are very weak. This is different from the $Ga_{1-x}In_xAs$ case, which would be related to the difference of the stabilities of the single crystals between two systems. $Zn_{1-x}Mn_xTe$ can form the single crystal in almost the whole zinc-blende crystal range about $0 \leq x \leq 0.7$,[24] while $Ga_{1-x}In_xAs$ only a few % near the end members of GaAs and InAs. It can be speculated that the local tetrahedral structure around the anions and cations in $Zn_{1-x}Mn_xTe$ would be much more flexible than those in $Ga_{1-x}In_xAs$, which may result in the larger atomic displacements. In fact, much smaller values of the bond stretching and bending force constants, 28.5 and 4.4 N/m for ZnTe[25] in contrast to 96–97 and 6–10 N/m for GaInAs,[9] respectively, were reported from Raman scattering and ultrasonic sound velocity measurements on the ZnTe crystal, which might support this speculation. The previous XAFS experiments on $Zn_{1-x}Mn_xTe$,[2] or even $Cd_{1-x}Mn_xTe$,[13,14] have, unfortunately, no detailed second-neighbor analyses such as $Ga_{1-x}In_xAs$ mixed crystals. For the further discussion, detailed measurements and analyses of XAFS as well as XD on the $Zn_{1-x}Mn_xTe$ mixed crystal are necessary to examine it.

As mentioned above, many models and ideas were proposed for bridging between the local structure clarified by XAFS and the long distant periodicity obtained by ordinary XD. Up to now, to our knowledge, the established structural information would be still limited to the local structures, e.g., the shape of the tetrahedron in the present zinc-blende cases, or the distortion of the large periodicity which can be detected by e.g., diffuse scattering,[9] and the information in the intermediate range between them is still unclear or a no man's land. Although the spatial resolution of the XFH is still poor, the present experiment on $Zn_{1-x}Mn_xTe$ diluted magnetic semiconductor or the previous one on the $Ga_{1-x}In_xSb$ mixed crystal[26] surely gives useful information on lattice distortions from the VCA crystal in the intermediate spatial range. The use of incident x-rays of high-energy and high-intensity from new generation synchrotron radiation facilities can significantly improve the spatial resolution of the XFH images. Also, the resolution and reliability of the XFH technique can be improved by developing the algorithm for the reconstructing 3D atomic images.[27] In the near future, it would become possible to observe the randomness of any constituent atoms at any neighboring shells with almost the same experimental errors from 3D XFH atomic images. In addition, theoretical investigations are also helpful to understand the lattice distortions in the intermediate range, as Zunger and co-workers[28–30] largely contributed by calculating accurate band structures and thermodynamic properties in the mixed crystals. An *ab initio* molecular dynamic simulation would be a powerful tool to understand the intermediate structure and the corresponding electronic properties of the mixed crystals, which would be useful for many applicational aims.

V. CONCLUSION

In conclusion, the present XFH measurement has successfully observed the lattice distortion in the $Zn_{1-x}Mn_xTe$ crystal in the intermediate range, and built bridges between the relatively *farsighted* XD and the relatively *nearsighted* XAFS measurements, which had shown an intrinsic difference even on the first neighbor distance in mixed crystals. The lattice distortions by mixing the element almost vanish within the five chemical bonds in this mixed crystal. The present result may not be specific only in $Zn_{1-x}Mn_xTe$ diluted magnetic semiconductor, but similar local lattice distortions would be present in any mixed crystals although the magnitudes of the sublattice distortion may be different.

ACKNOWLEDGMENTS

The authors acknowledge S. Sasaki for the encouragement and support for this study. The XFH experiments were performed at the beamline BL6C in the PF-KEK (Proposals No. 2005G127 and No. 2007G567). This work was supported by the Grant-in-Aid for Scientific Research from the Ministry of Education, Culture, Sports, Science, and Technology of Japan.

*hosokawa@cc.it-hiroshima.ac.jp

[1] J. K. Furdyna, W. Giriat, D. F. Mitchell, and G. I. Sproule, J. Solid State Chem. **46**, 349 (1983).
[2] N. Happo, H. Sato, T. Mihara, K. Mimura, S. Hosokawa, Y. Ueda, and M. Taniguchi, J. Phys.: Condens. Matter **8**, 4315 (1996).
[3] L. Vegard, Z. Phys. **5**, 17 (1921).
[4] L. Pauling, *The Nature of the Chemical Bonds* (Cornell University Press, New York, 1967).
[5] I. Yonenaga and M. Sakurai, Phys. Rev. B **64**, 113206 (2001).
[6] J. C. Mikkelsen, Jr. and J. B. Boyce, Phys. Rev. Lett. **49**, 1412 (1982).
[7] J. C. Mikkelsen, Jr. and J. B. Boyce, Phys. Rev. B **28**, 7130 (1983).
[8] V. Petkov, I.-K. Jeong, J. S. Chung, M. F. Thorpe, S. Kycia, and S. J. L. Billinge, Phys. Rev. Lett. **83**, 4089 (1999).
[9] I.-K. Jeong, F. Mohiuddin-Jacobs, V. Petkov, S. J. L. Billinge, and S. Kycia, Phys. Rev. B **63**, 205202 (2001).
[10] J. B. Boyce and J. C. Mikkelsen, Jr., J. Cryst. Growth **98**, 37 (1989).
[11] J. Pellicer-Porres, A. Polian, A. Segura, V. Muñoz-Sanjosé, A. Di Cicco, and A. Traverse, J. Appl. Phys. **96**, 1491 (2004).
[12] N. Motta, A. Balzarotti, P. Letardi, A. Kisiel, M. T. Czyżyk, M. Zimnal-Starnawska, and M. Podogòrny, J. Cryst. Growth **72**, 205 (1985).
[13] A. Balzarotti, M. Czyżyk, A. Kisiel, N. Motta, M. Podgòrny, and M. Zimnal-Starnawska, Phys. Rev. B **30**, 2295 (1984).
[14] A. Balzarotti, N. Motta, A. Kisiel, M. Zimnal-Starnawska, M. T. Czyżyk, and M. Podgòrny, Phys. Rev. B **31**, 7526 (1985).
[15] J. B. Boyce and J. C. Mikkelsen, Jr., Phys. Rev. B **31**, 6903 (1985).
[16] A. Di Cicco, E. Principi, and A. Filipponi, Phys. Rev. B **65**, 212106 (2002).
[17] M. Tegze and G. Faigel, Nature (London) **380**, 49 (1996).
[18] M. Tegze, G. Faigel, S. Marchesini, M. Belakhovsky, and O. Ulrich, Nature (London) **407**, 38 (2000).
[19] K. Hayashi, in *Advances in Imaging and Electron Physics*, edited by P. W. Hawkes (Academic, New York, 2006), Vol. 140, p. 120.
[20] K. Hayashi, Y. Takahashi, E. Matsubara, S. Kishimoto, T. Mori, and M. Tanaka, Nucl. Instrum. Methods Phys. Res. B **196**, 180 (2002).
[21] J. J. Barton, Phys. Rev. Lett. **67**, 3106 (1991).
[22] S. Hosokawa, N. Happo, and K. Hayashi, J. Magn. Magn. Mater. **310**, 2707 (2007).
[23] A. L. Ankudinov, B. Ravel, J. J. Rehr, and S. D. Conradson, Phys. Rev. B **58**, 7565 (1998).
[24] *Diluted Magnetic Semiconductors in Semiconductors and Semimetals*, edited by J. K. Furdyna and J. Kossut (Academic, New York, 1988), Vol. 25.
[25] E. N. Prykina, Yu. I. Polygalov, and A. V. Kopytov, Fiz. Tekh. Poluprovodn. **35**, 89 (2001) [Semiconductors **35**, 91 (2001)].
[26] S. Hosokawa, T. Ozaki, N. Takata, N. Happo, H. Ikemoto, T. Shishido, and K. Hayashi, J. Cryst. Growth **311**, 978 (2009).
[27] T. Matsushita, F. Z. Guo, M. Suzuki, F. Matsui, H. Daimon, and K. Hayashi, Phys. Rev. B **78**, 144111 (2008).
[28] A. Zunger and J. E. Jaffe, Phys. Rev. Lett. **51**, 662 (1983).
[29] S.-H. Wei and A. Zunger, Phys. Rev. B **35**, 2340 (1987).
[30] A. Zunger, S.-H. Wei, L. G. Ferreira, and J. E. Bernard, Phys. Rev. Lett. **65**, 353 (1990).